Supplement of Atmos. Chem. Phys., 25, 12629–12656, 2025
https://doi.org/10.5194/acp-25-12629-2025-supplement

Atmospheric Chemistry and Physics Open Access

Supplement of

A diagnostic intercomparison of modeled ozone dry deposition over North America and Europe using AQMEII4 regional-scale simulations

Christian Hogrefe et al.

Correspondence to: Christian Hogrefe (hogrefe.christian@epa.gov)

Table of Contents

Table S1: WRF/CMAQ STAGE mapping of the dry deposition module LU categories (AQMEII4) from the LSM LU categories (MODIS product MCD12Q1v6 for 2017 (Friedl and Sulla-Menashe, 2019) for the U.S. EPA simulations over North America, MODIS (Friedl et al., 2002) + extended urban categories over the greater London area for the University of Hertfordshire simulations over Europe)

Dry Deposition LU	LSM LU
1: Water	17: water
2: Developed / Urban	13: Urban and Built-up Additional urban categories over the greater London area for the University of Hertfordshire WRF/CMAQ STAGE simulations
3: Barren	16: Barren or Sparsely Vegetated
4: Evergreen needleleaf forest	1: Evergreen Needleleaf Forest
5: Deciduous needleleaf forest	3: Deciduous Needleleaf Forest
6: Evergreen broadleaf forest	2: Evergreen Broadleaf Forest
7: Deciduous broadleaf forest	4: Deciduous Broadleaf Forest
8: Mixed forest	5: Mixed Forest
9: Shrubland	6: Closed Shrublands; 7: Open Shrublands
10: Herbaceous	N/A
11: Planted / Cultivated	12: Croplands 14: Cropland-Natural Vegetation Mosaic
12: Grassland	10: Grasslands
13: Savanna	8: Woody Savanna 9: Savanna
14: Wetlands	11: Permanent Wetlands
15: Tundra	18: Wooded Tundra 19: Mixed Tundra 20: Barren Tundra
16: Snow and Ice	15: Snow and Ice

Table S2. GEM-MACH (Base) and GEM-MACH (Ops) mapping of the dry deposition module LU categories (Makar et al., 2018) from the LSM LU categories (Zhang et al., 2003)

Dry Deposition LU	LSM LU
1: Evergreen needleleaf forest	4: Evergreen needleleaf trees
2: Evergreen broadleaf forest	5: Evergreen broadleaf trees 8: Tropical broadleaf trees
3: Deciduous needleleaf forest	6: Deciduous needleleaf trees
4: Deciduous broadleaf forest	7: Deciduous broadleaf trees 9: Drought deciduous trees
5: Mixed Forest	25: Mixed Wood Forest
6: Grassland	14: Long grass
7: Crops, mixed farming	15:Crops 17: Sugar 18: Maize 19: Cotton 20: Irrigated Crops
8: Desert	24: Desert
9: Tundra	22: Tundra
10: Dwarf trees, shrubs	10: Evergreen broadleaf shrubs 11: Deciduous shrubs 12: Thorn shrubs 13: Short grass and forbs 26: Mixed Shrubs
11: Wetland with plants	22: Swamp
12: Ice caps and glaciers	2: Ice
13: Inland water	3: Inland Lake (Fresh)
14: Ocean	1: Water (Ocean)
15: Urban	21: Urban

Table S3. WRF/Chem (RIFS) mapping of the dry deposition module LU categories (USGS24) from the LSM LU categories for the EUR domain (Coordination of Information on the Environment (CORINE) Land Cover, EEA 2020)

Dry Deposition LU	LSM LU
1: Urban and Built-Up Land	31: Low Intensity Residential 32: High Intensity Residential 33: Industrial or Commercial
2: Dryland Cropland and Pasture	2: Dryland Cropland and Pasture
3: Irrigated Cropland and Pasture	3: Irrigated Cropland and Pasture;
4: Mixed Dryland/Irrigated Cropland and Pasture	4: Mixed Dryland/Irrigated Cropland and Pasture
5: Cropland / Grassland Mosaic	5: Cropland/Grassland Mosaic;
6: Cropland / Woodland Mosaic	6: Cropland/Woodland Mosaic
7: Grassland	7: Grassland
8: Shrubland	8: Shrubland
9: Mixed Shrubland / Grassland	9: Mixed Shrubland / Grassland
10: Savanna	10: Savanna
11: Deciduous Broadleaf Forest	11: Deciduous Broadleaf Forest
12: Deciduous Needleleaf Forest	12: Deciduous Needleleaf Forest
13: Evergreen Broadleaf Forest	13: Evergreen Broadleaf Forest
14: Evergreen Needleleaf Forest	14: Evergreen Needleleaf Forest
15: Mixed Forest	15: Mixed Forest
16: Water Bodies	16: Water Bodies
17: Herbaceous Wetland	17: Herbaceous Wetland
18: Wooded Wetland	18: Wooded Wetland
19: Barren or Sparsely Vegetated	19: Barren or Sparsely Vegetated
20: Herbaceous Tundra	20: Herbaceous Tundra
21: Wooded Tundra	21: Wooded Tundra
22: Mixed Tundra	22: Mixed Tundra
23: Bare Ground Tundra	23: Bare Ground Tundra
24 Snow or Ice	24: Snow or Ice

Table S4: WRF/Chem (NCAR) mapping of the dry deposition module LU categories (USGS24) from the LSM LU categories (MODIS product MCD12Q1v5.1 as processed by Broxton et al., 2014)

Dry Deposition LU	LSM LU
1: Urban and Built-Up Land	13 Urban and Built-Up
2: Dryland Cropland and Pasture	N/A
3: Irrigated Cropland and Pasture	N/A
4: Mixed Dryland/Irrigated Cropland and Pasture	12 Croplands
5: Cropland / Grassland Mosaic	14 cropland/natural vegetation mosaic
6: Cropland / Woodland Mosaic	N/A
7: Grassland	10: Grasslands
8: Shrubland	6: Closed Shrublands
9: Mixed Shrubland / Grassland	7: Open Shrublands
10: Savanna	8: Woody Savannas 9: Savannas
11: Deciduous Broadleaf Forest	4: Deciduous Broadleaf Forest
12: Deciduous Needleleaf Forest	3: Deciduous Needleleaf Forest
13: Evergreen Broadleaf Forest	2: Evergreen Broadleaf Forest
14: Evergreen Needleleaf Forest	1: Evergreen Needleleaf Forest
15: Mixed Forest	5: Mixed Forests
16: Water Bodies	17: Water
17: Herbaceous Wetland	11: Permanent wetlands
18: Wooded Wetland	N/A
19: Barren or Sparsely Vegetated	16: Barren or Sparsely Vegetated 20: Barren Tundra
20: Herbaceous Tundra	N/A
21: Wooded Tundra	18: Wooded Tundra
22: Mixed Tundra	19: Mixed Tundra
23: Bare Ground Tundra	N/A
24: Snow or Ice	15: Snow and Ice

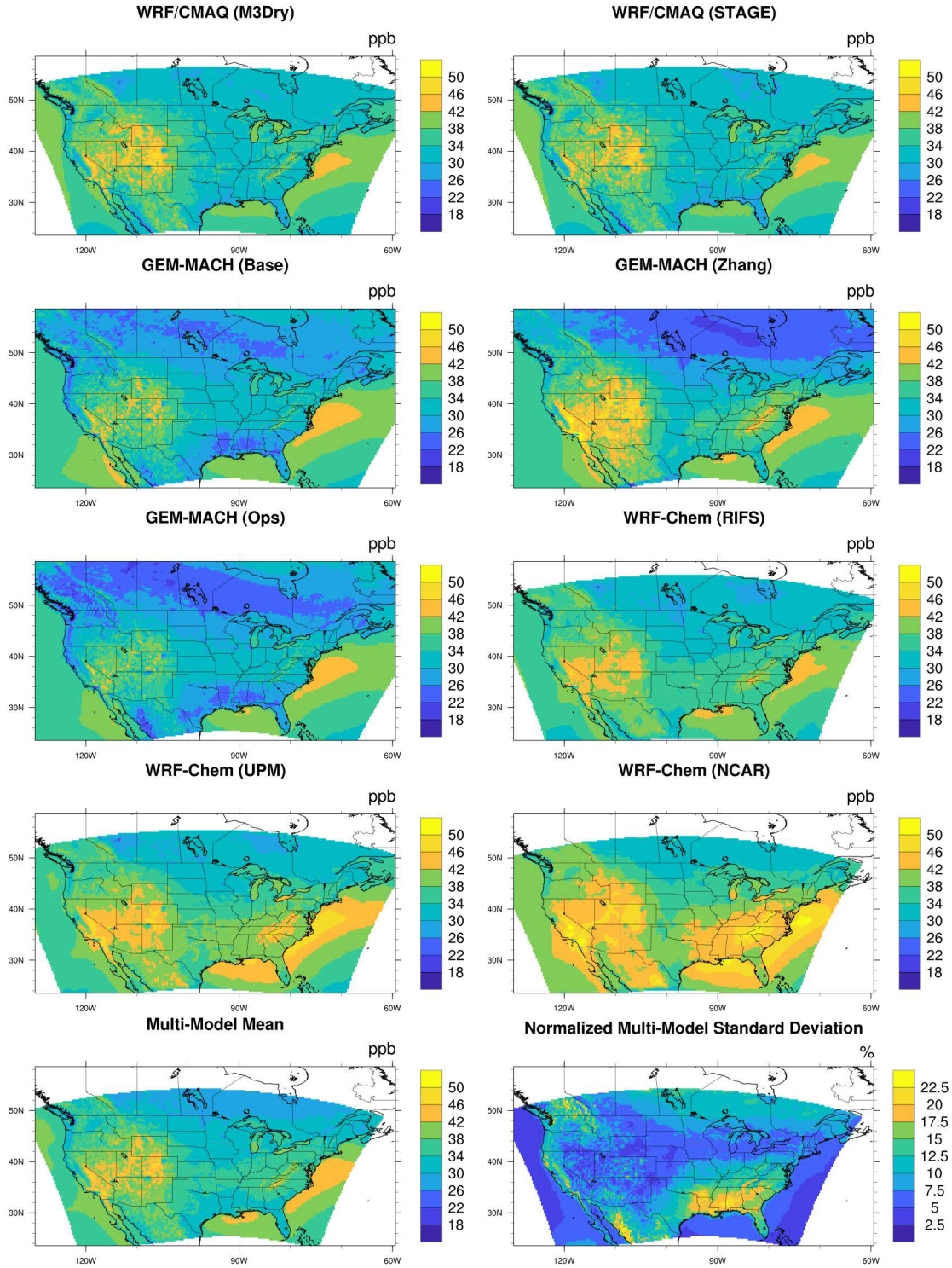

Figure S1: 2016 annual total O_3 mixing ratio (ppb) for each model, the multi-model mean, and the normalized multi-model standard deviation over the NA domain. Note that the plots for individual models are not clipped to the domain common to all simulations and show the maximum spatial extent submitted for each model. The multi-model mean and normalized standard deviations are calculated and shown over the common domain.

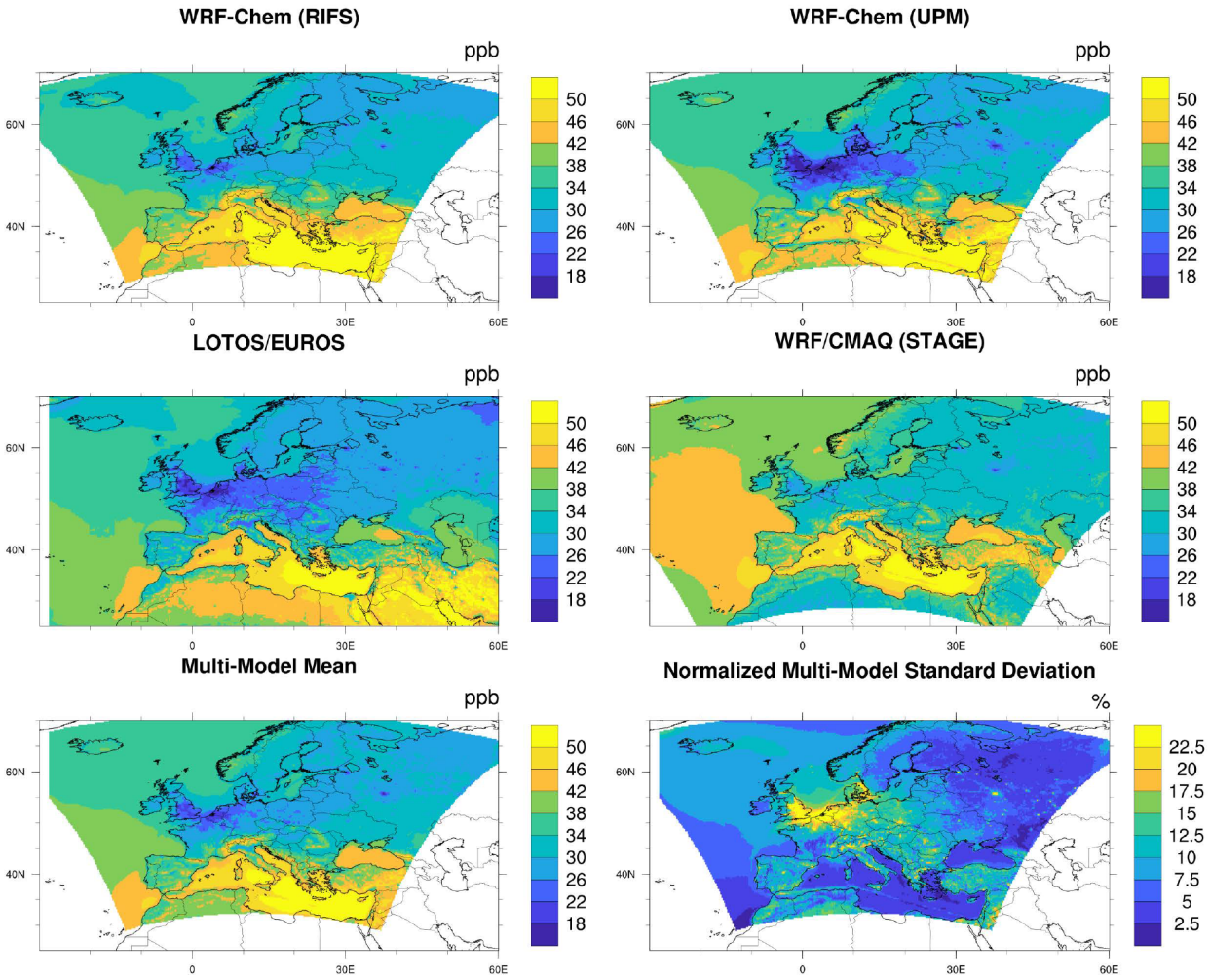

Figure S2: 2016 annual total O_3 mixing ratio (ppb) for each model, the multi-model mean, and the normalized multi-model standard deviation over the EUR domain. Note that the plots for individual models are not clipped to the domain common to all simulations and show the maximum spatial extent submitted for each model. The multi-model mean and normalized standard deviations are calculated and shown over the common domain.

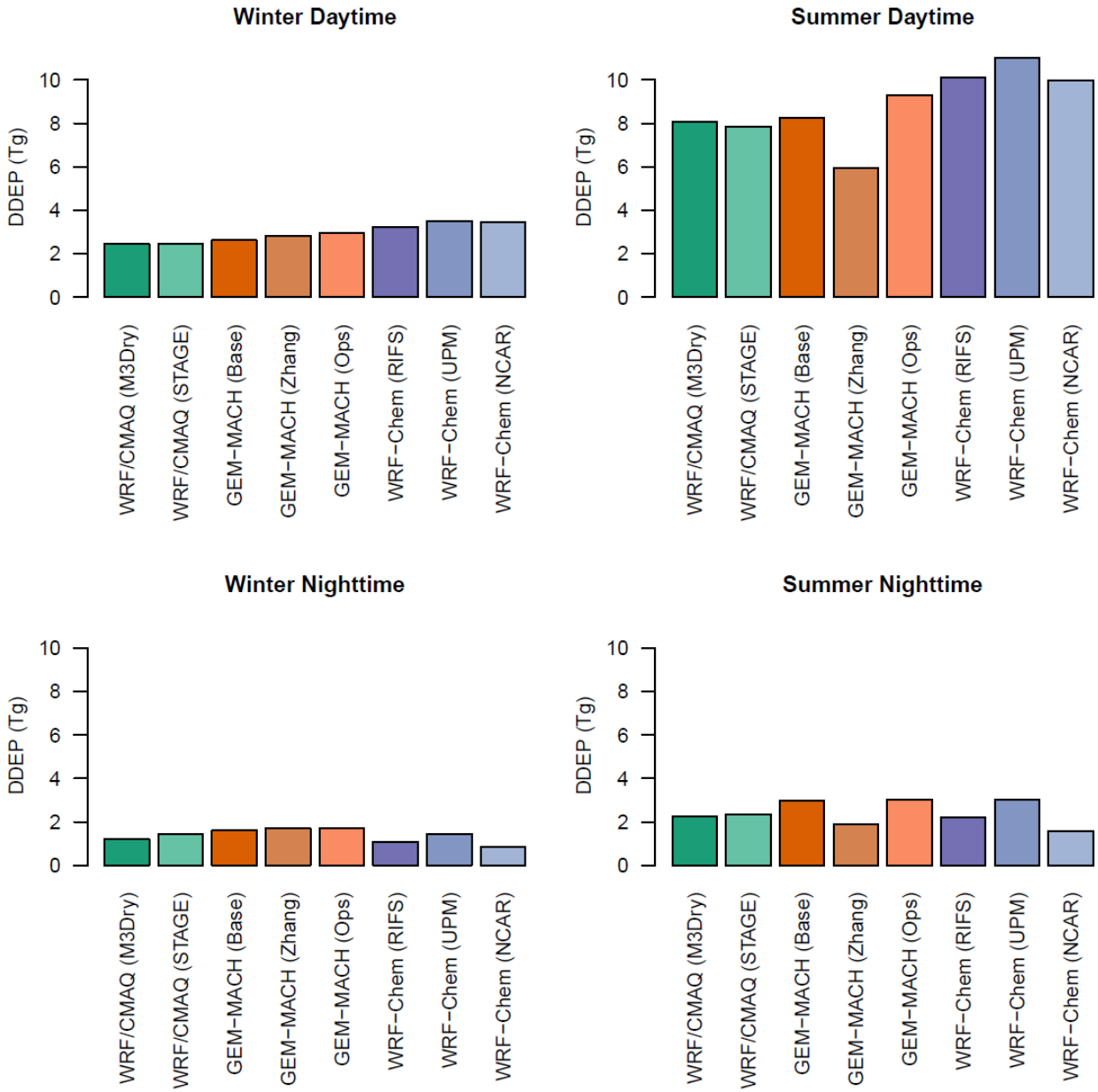

Figure S3: Seasonal and diurnal variations in 2016 NA domain total O_3 grid-scale dry deposition fluxes (in Tg). Totals are calculated over all non-water grid cells in the analysis domain common to all models. Daytime values are calculated from 10:00 LST to 14:00 LST while nighttime values are calculated from 22:00 LST to 02:00 LST. a) winter daytime, b) summer daytime, c) winter nighttime, d) summer nighttime

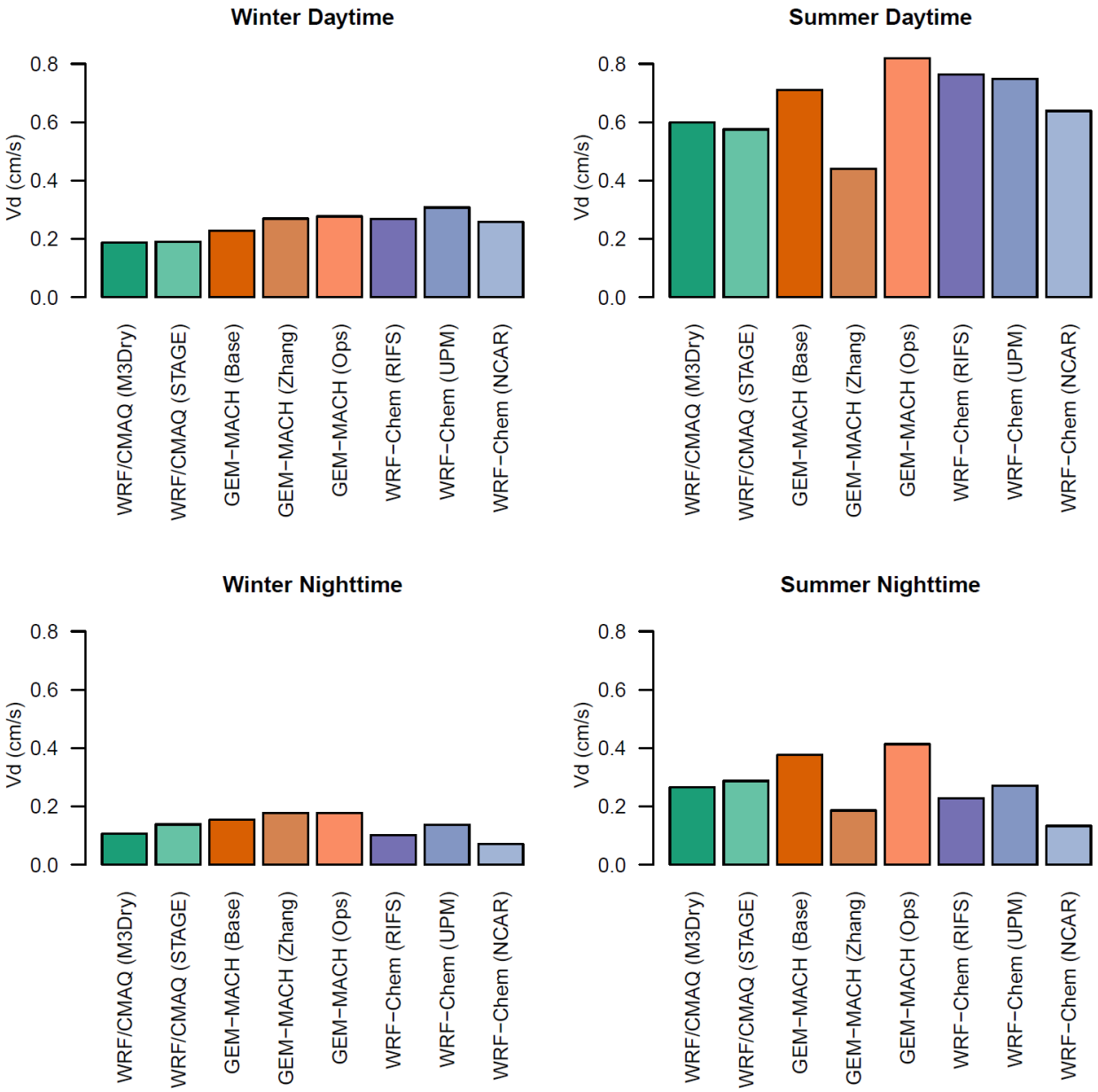

Figure S4: Seasonal and diurnal variations in 2016 NA domain average O_3 grid-scale dry deposition velocities (in cm/s). Averages are calculated over all non-water grid cells in the analysis domain common to all models. Daytime values are calculated from 10:00 LST to 14:00 LST while nighttime values are calculated from 22:00 LST to 02:00 LST. a) winter daytime, b) summer daytime, c) winter nighttime, d) summer nighttime

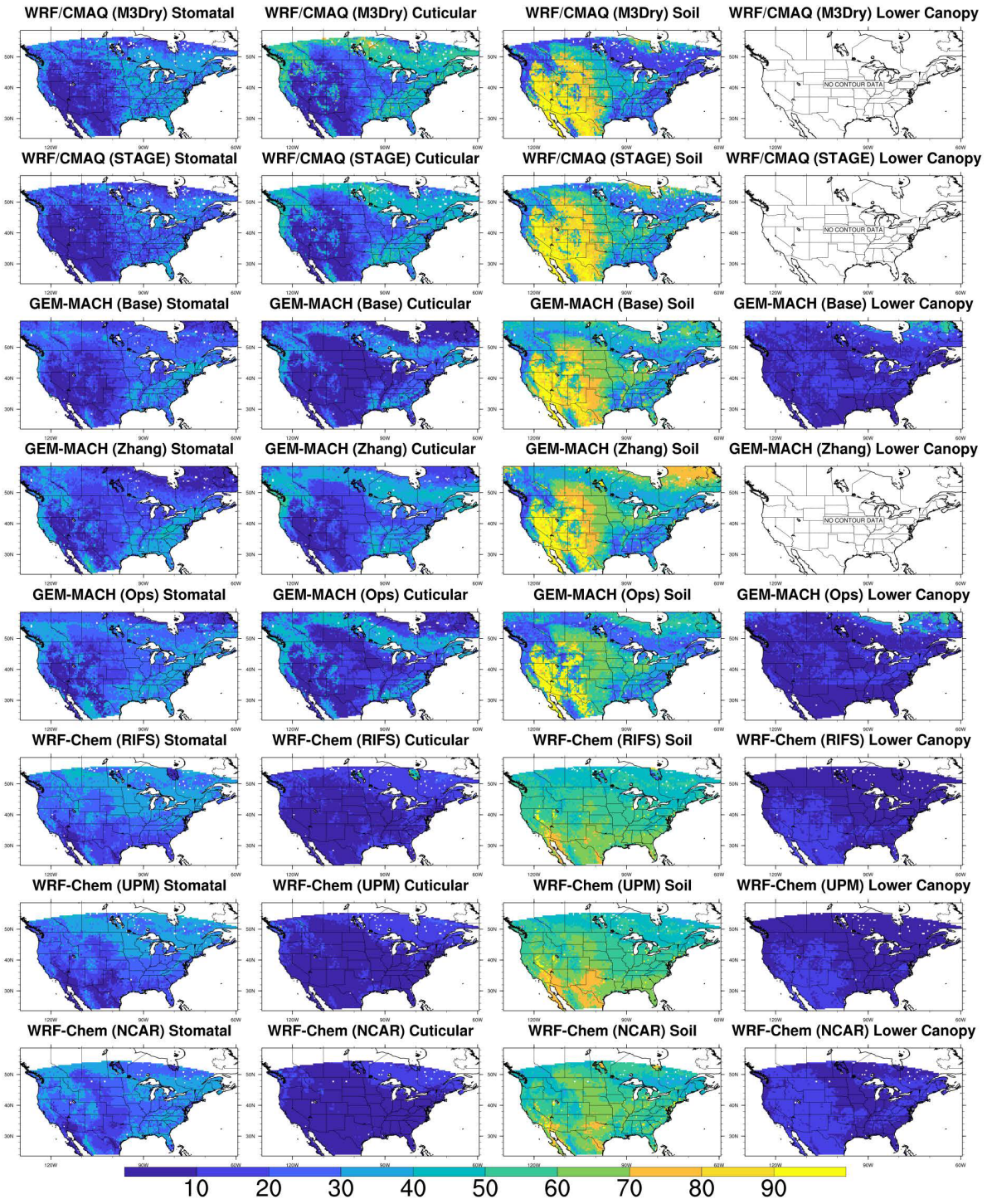

Figure S5: Percentage contributions of grid-scale ozone effective conductances to the sum of all pathways, averaged over the entire year. Results are for the NA domain during 2016. Note that these maps are not clipped to the domain common to all simulations and show the maximum spatial extent of non-water cells submitted for each model.

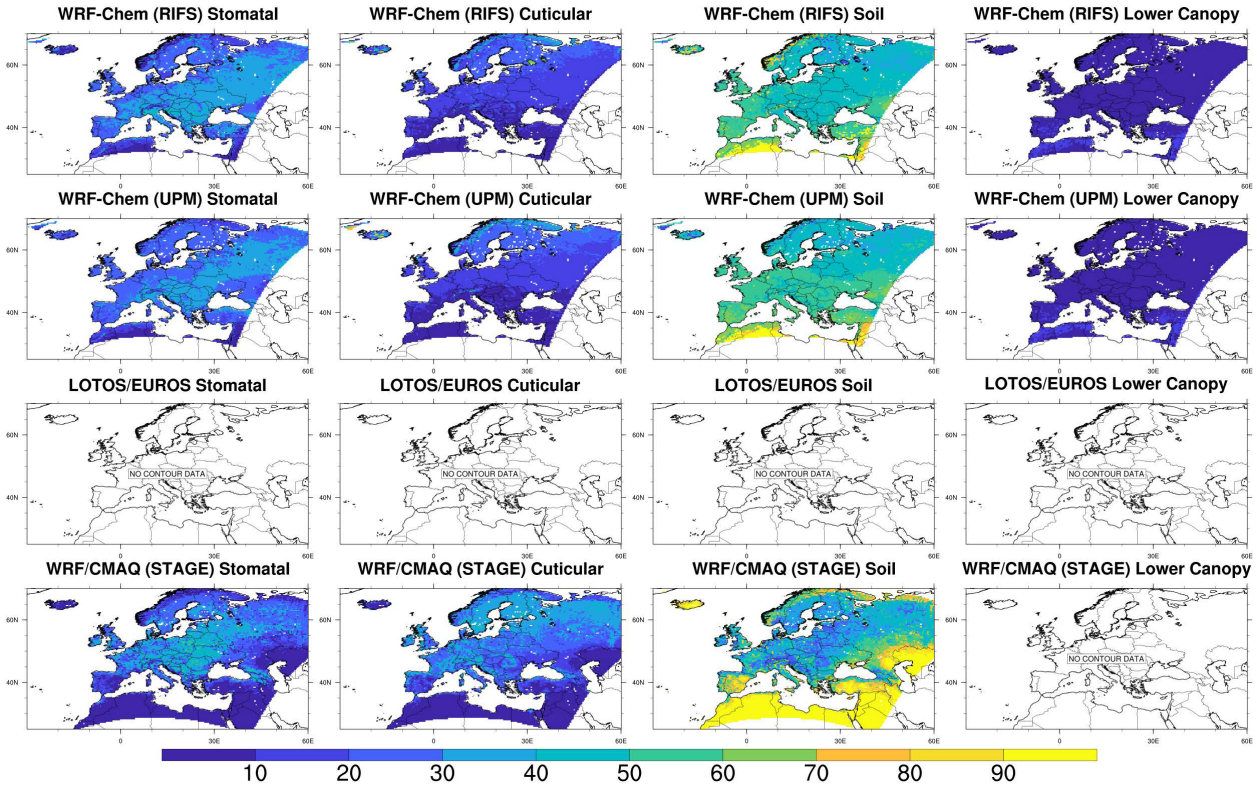

Figure S6: Percentage contributions of grid-scale ozone effective conductances to the sum of all pathways, averaged over the entire year. Results are for the EUR domain during 2010. Note that these maps are not clipped to the domain common to all simulations and show the maximum spatial extent of non-water cells submitted for each model.

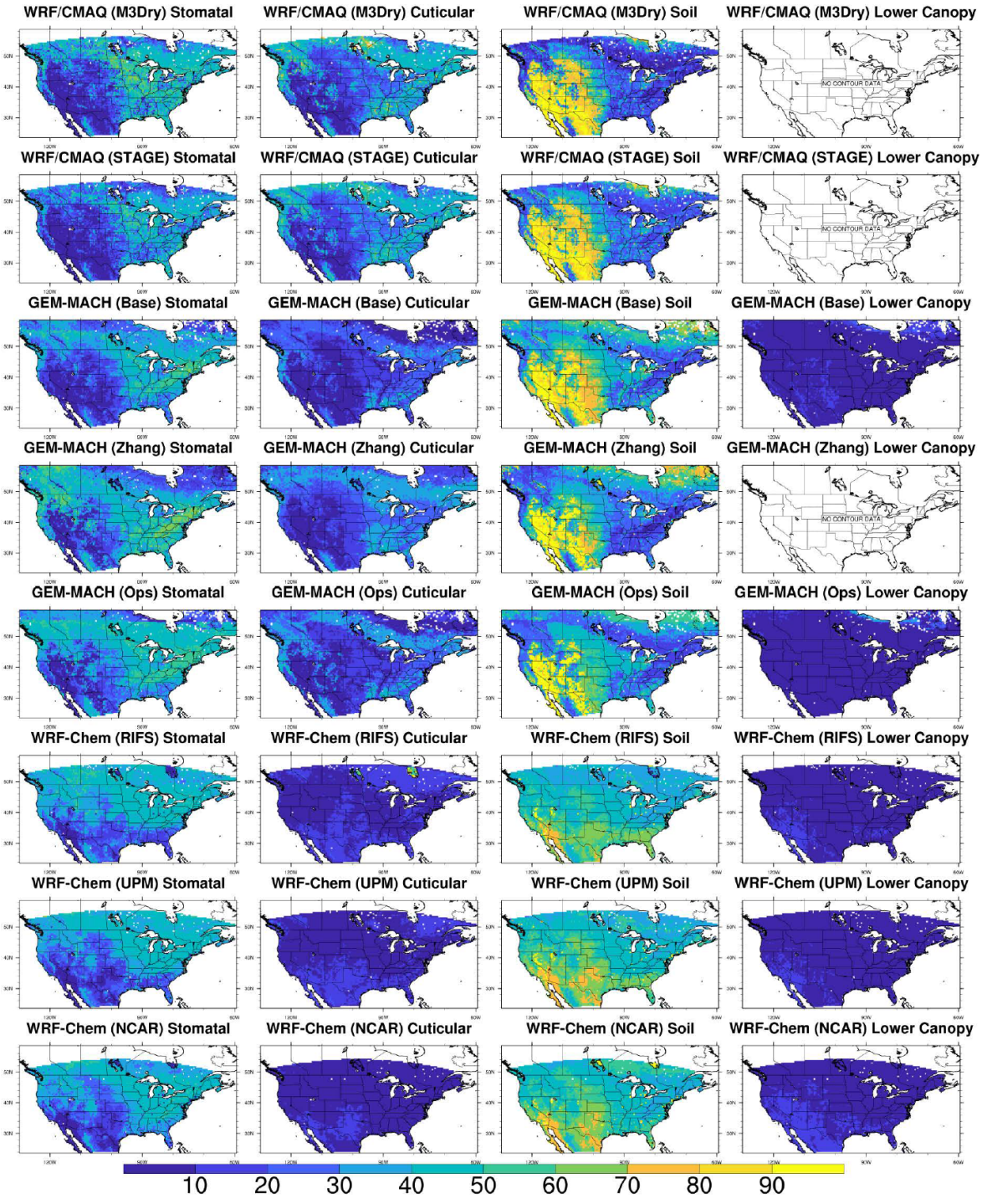

Figure S7. Percentage contributions of grid-scale ozone effective conductances to the sum of all pathways, averaged over all hours during summer. Results are for the NA domain during 2016. Note that these maps are not clipped to the domain common to all simulations and show the maximum spatial extent of non-water cells submitted for each model.

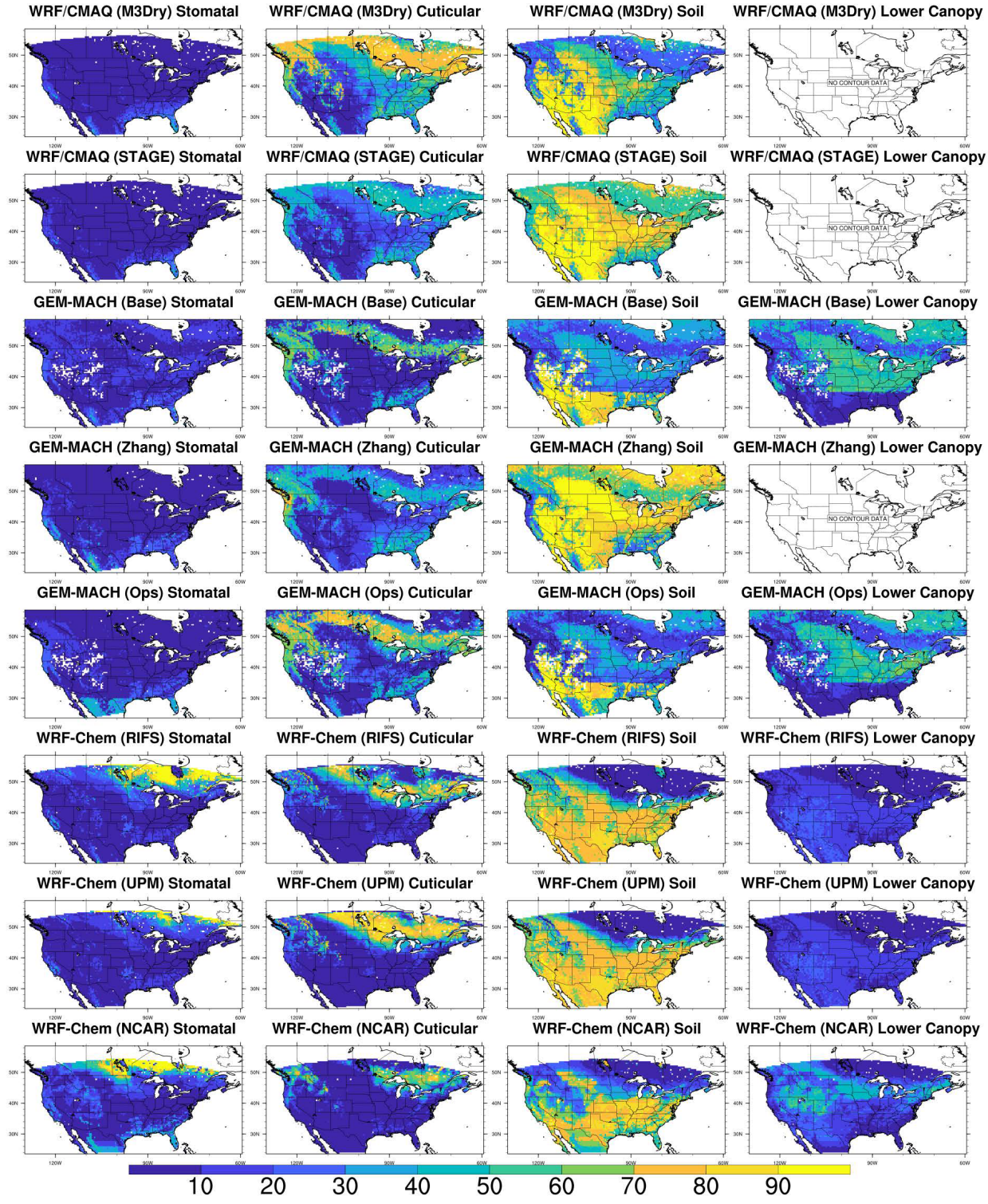

Figure S8: As in Figure S5 but for winter.

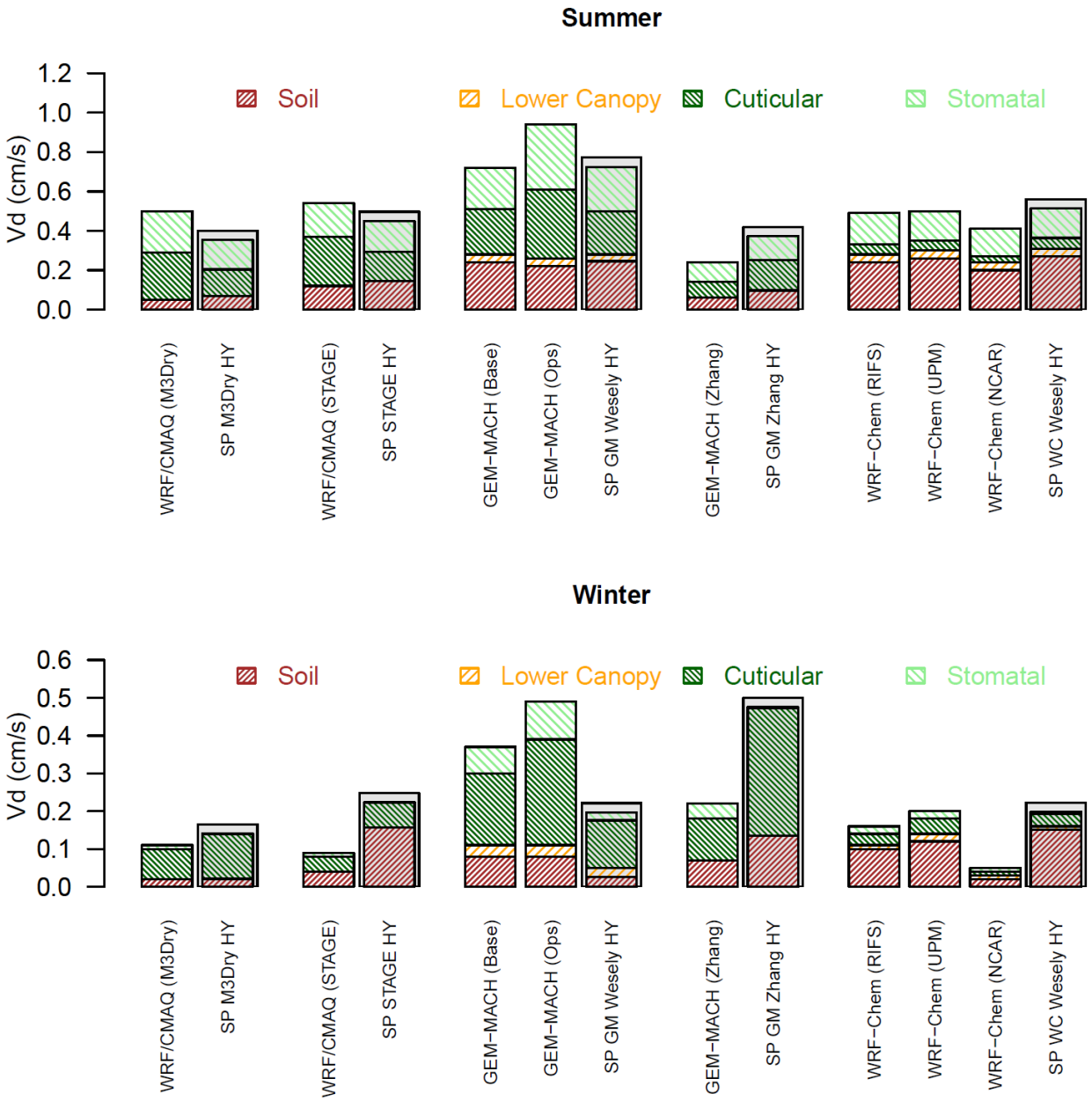

Figure S9: Summer and winter effective conductances and ozone deposition velocities calculated by the grid models for evergreen needleleaf forest grid cells and calculated by the corresponding subset of single point (SP) models analyzed in Clifton et al. (2023) at the Hyytiälä (HY) site. In the x-axis labels, results for the SP GEM-MACH Wesely and Zhang simulations are shown as "SP GM Wesely" and "SP GM Zhang", respectively, while results for the SP WRF-Chem Wesely simulations are shown as "SP WC Wesely". The evergreen needleleaf forest grid cells selected for this analysis are those in which a given model had at least 85% coverage for this LU category. The number of these grid cells differs across models due to underlying differences in LU (see Section 3.3).

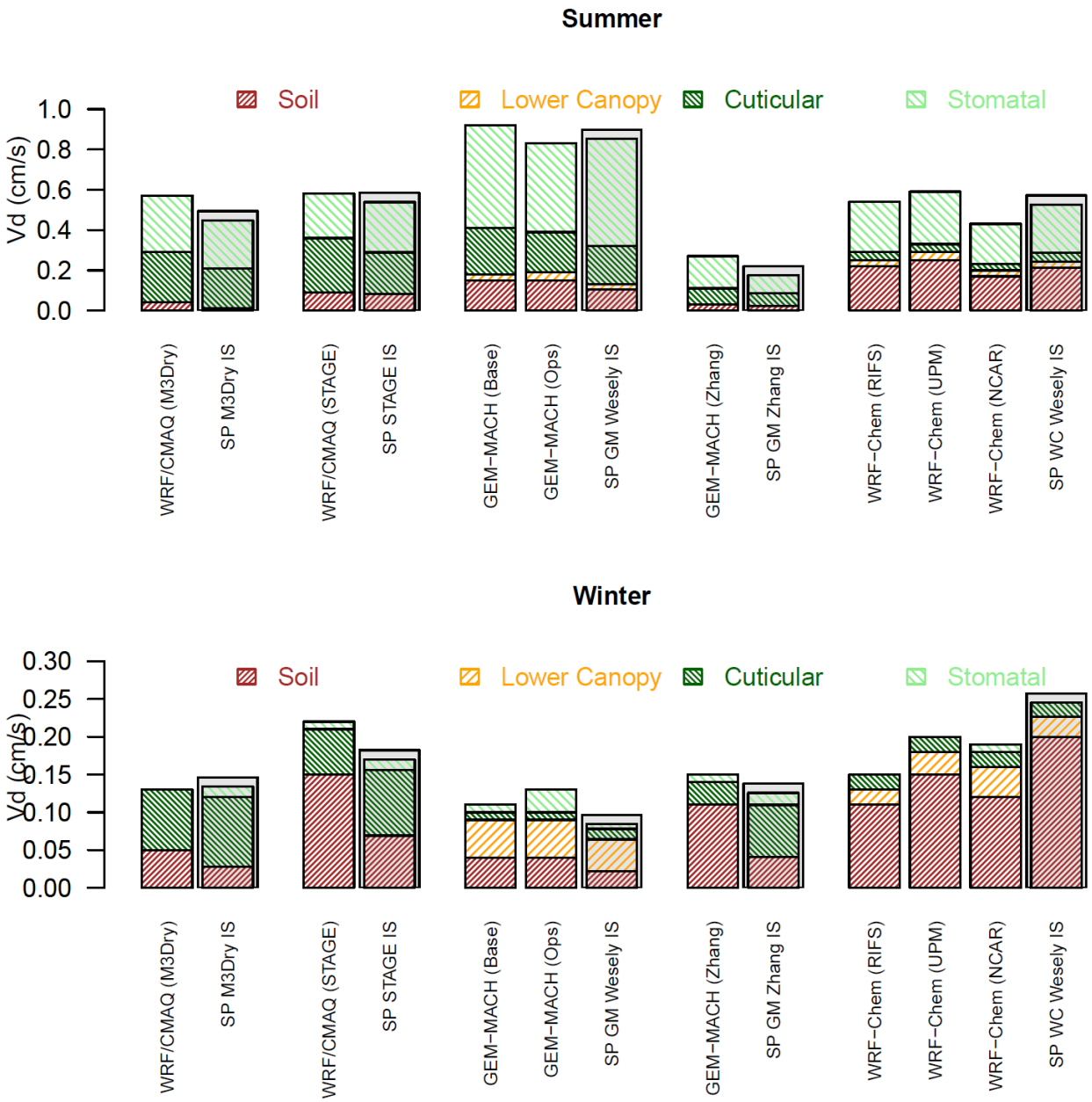

Figure S10: Summer and winter effective conductances and ozone deposition velocities calculated by the grid models for deciduous broadleaf forest grid cells and calculated by the corresponding subset of single point (SP) models analyzed in Clifton et al. (2023) at the Ispra (IS) site. In the x-axis labels, results for the SP GEM-MACH Wesely and Zhang simulations are shown as "SP GM Wesely" and "SP GM Zhang", respectively, while results for the SP WRF-Chem Wesely simulations are shown as "SP WC Wesely". The deciduous broadleaf forest grid cells selected for this analysis are those in which a given model had at least 85% coverage for this LU category. The number of these grid cells differs across models due to underlying differences in LU (see Section 3.3).

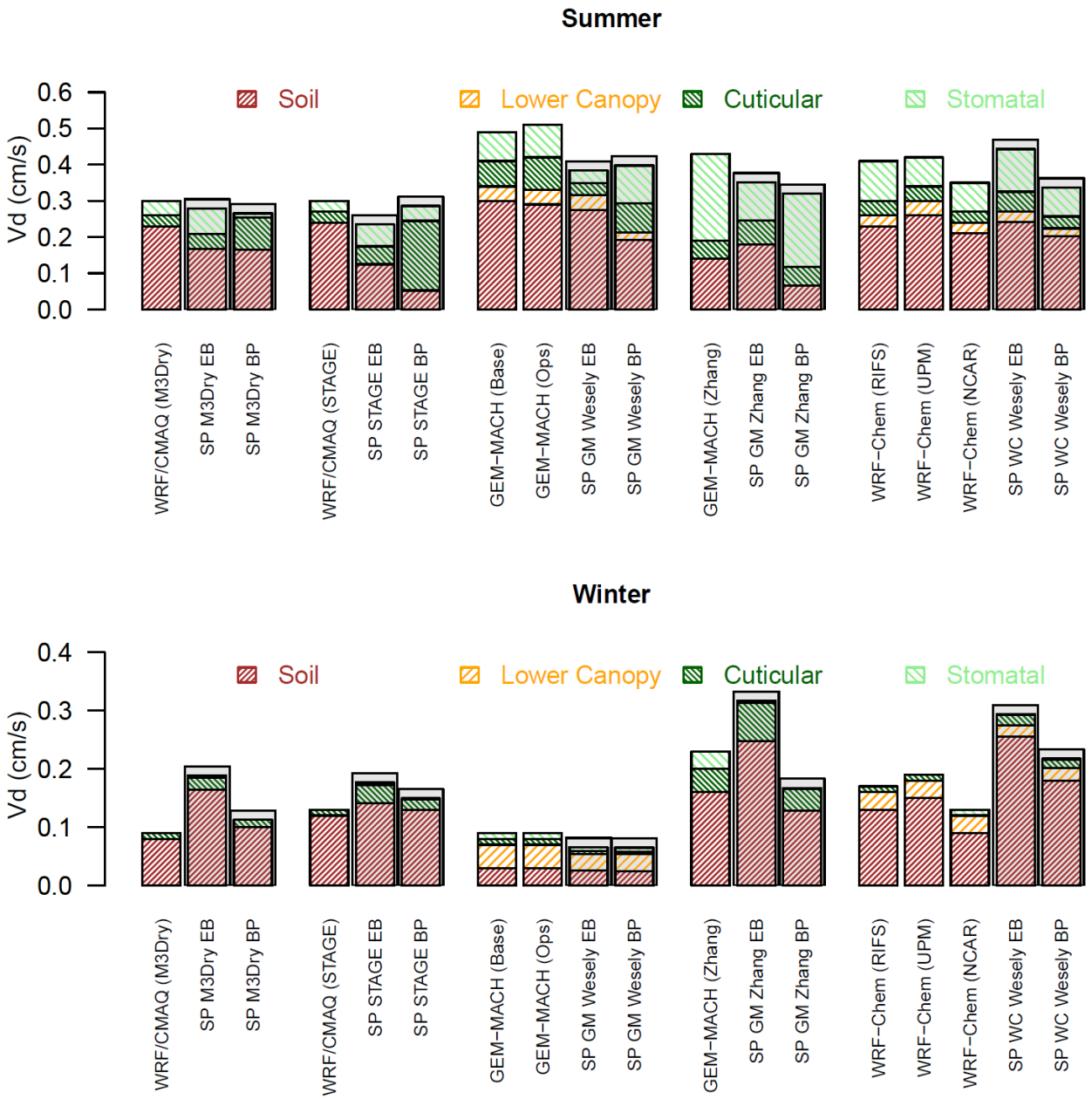

Figure S11: Summer and winter effective conductances and ozone deposition velocities calculated by the grid models for grassland grid cells and calculated by the corresponding subset of single point (SP) models analyzed in Clifton et al. (2023) at the Easter Bush (EB) and Bugacpuszta (BP) sites. In the x-axis labels, results for the SP GEM-MACH Wesely and Zhang simulations are shown as "SP GM Wesely" and "SP GM Zhang", respectively, while results for the SP WRF-Chem Wesely simulations are shown as "SP WC Wesely". The grassland grid cells selected for this analysis are those in which a given model had at least 85% coverage for this LU category. The number of these grid cells differs across models due to underlying differences in LU (see Section 3.3).

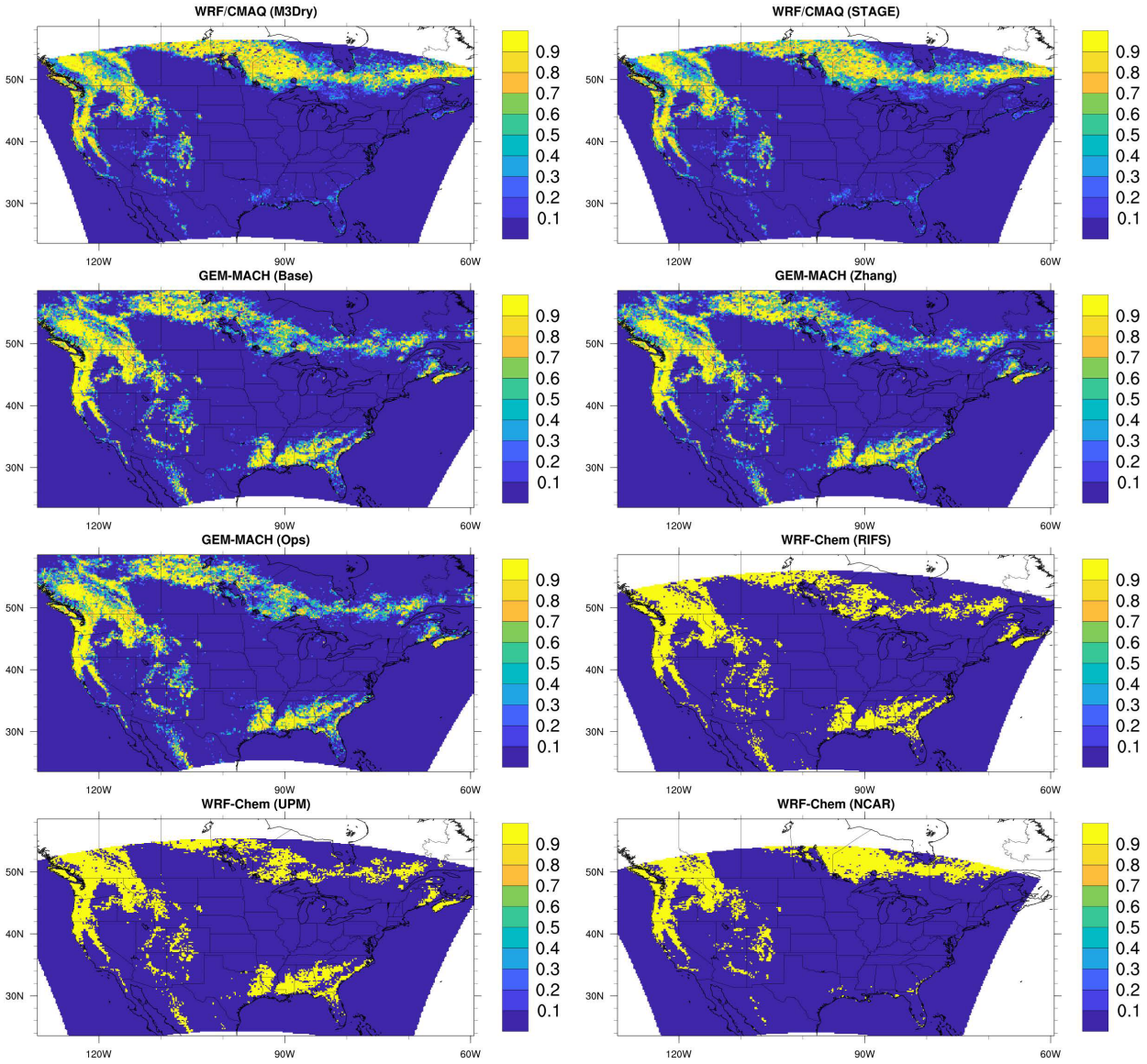

Figure S12: Fractional coverage of the evergreen needleleaf forest LU category for each of the participating models over the NA domain.

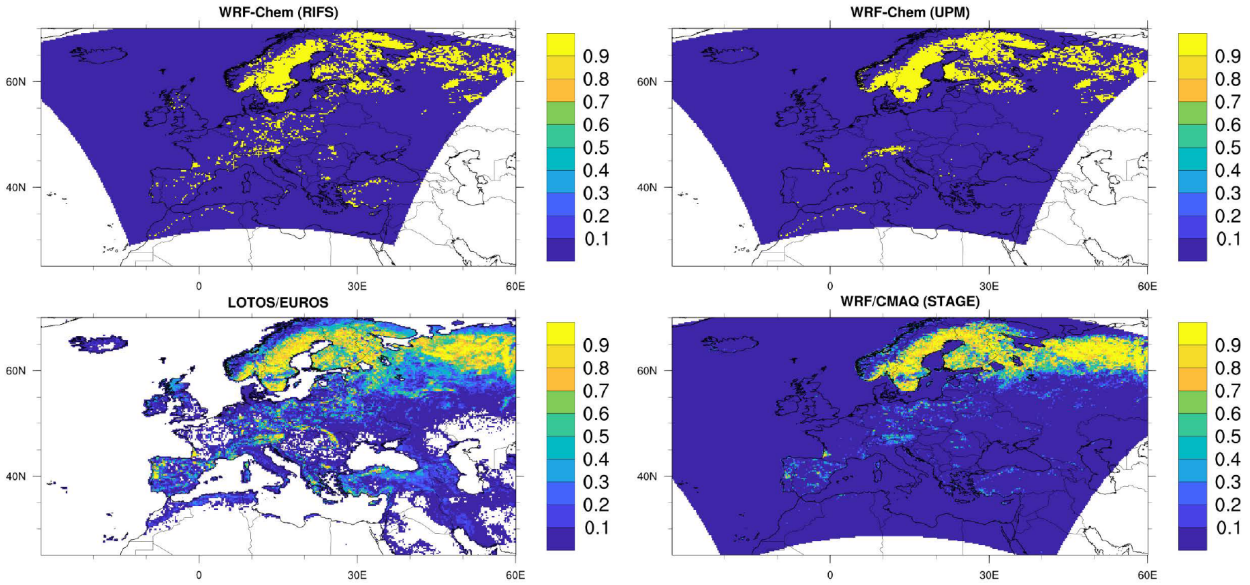

Figure S13: Fractional coverage of the evergreen needleleaf forest LU category for each of the participating models over the EUR domain.

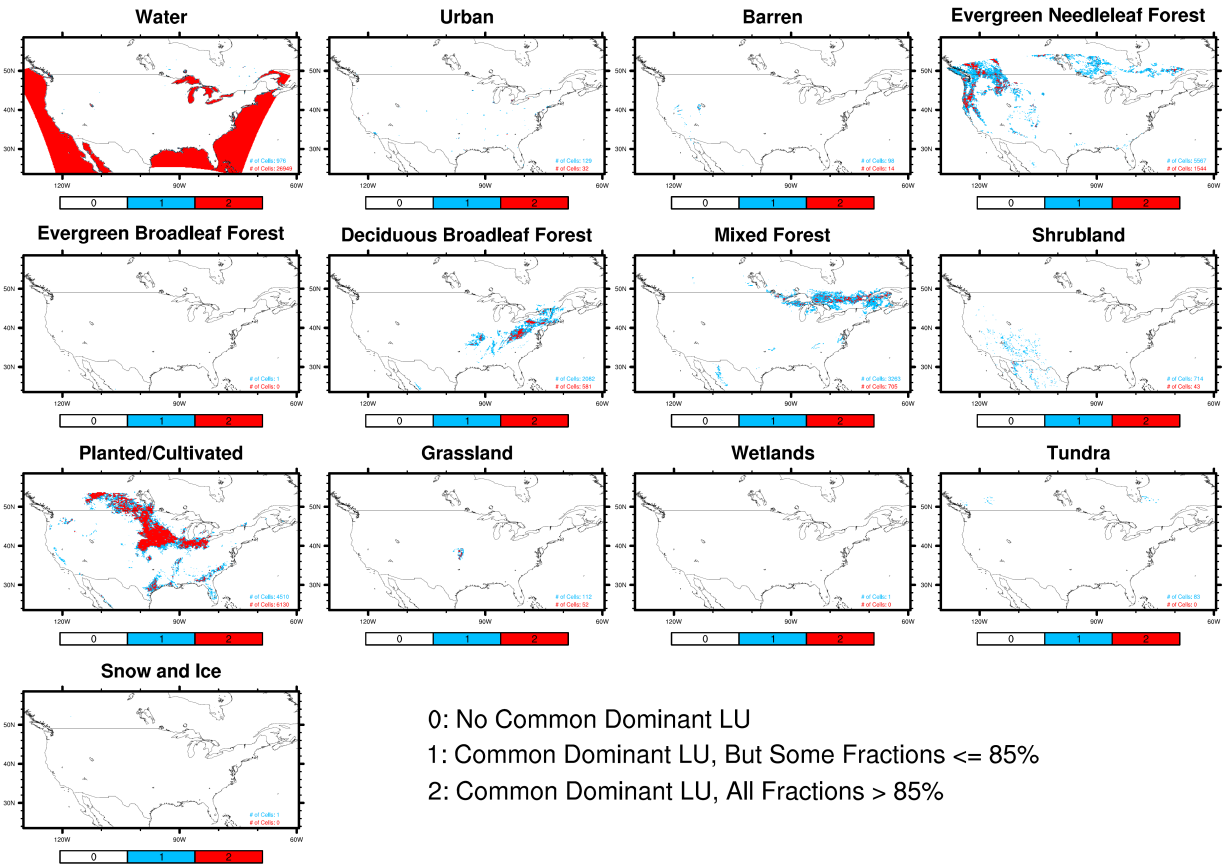

Figure S14: For each LU category, maps depicting the location of grid cells that i) do not share a common dominant LU category across models (white cells), ii) share a common dominant LU category across models but not all models have a fractional coverage > 85% for that LU category (blue cells), or iii) share a common dominant LU category across models and all models have a fractional coverage > 85% for that LU category (red). Results show are for the NA domain. The number of blue and red cells is shown as insert in each map. No maps are shown for the deciduous needleleaf forest, herbaceous, and savanna LU categories because there is not a single common dominant LU grid cell across models for these categories (see Table 5).

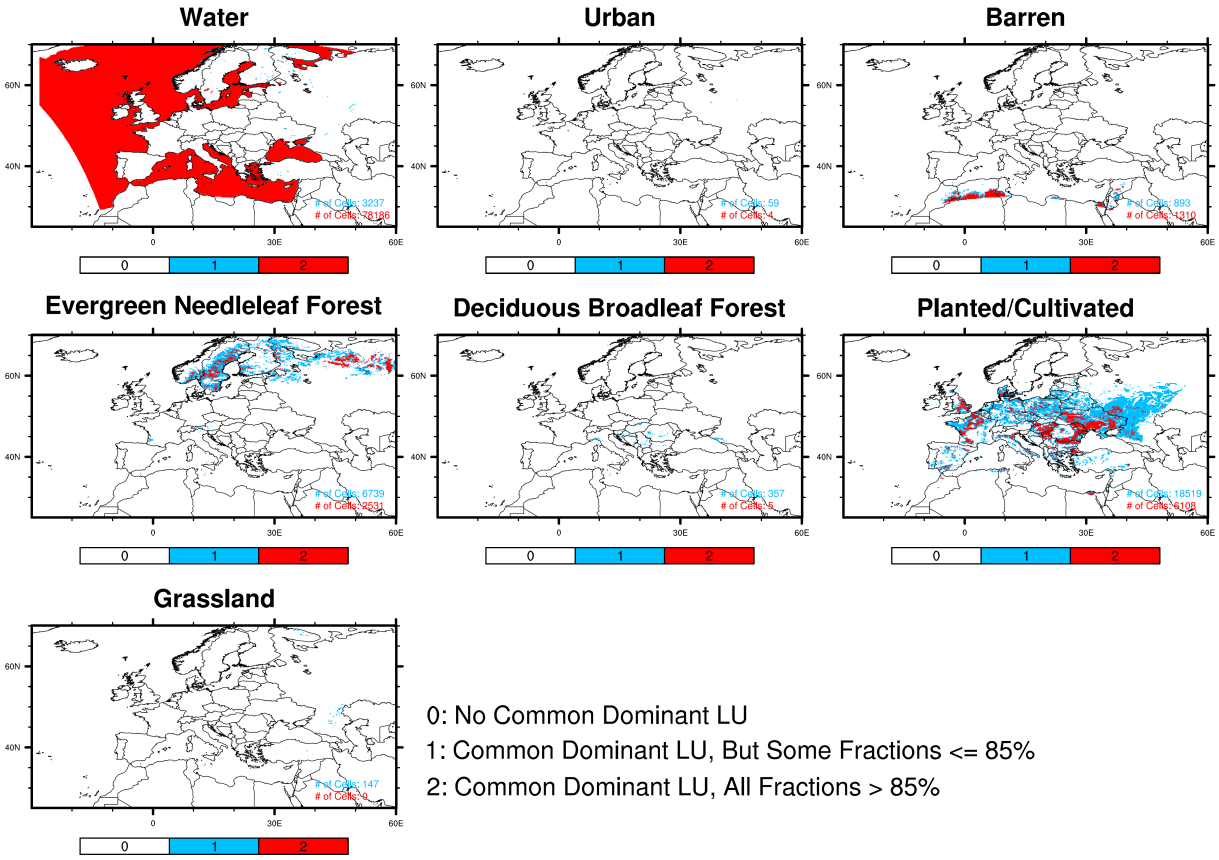

Figure S15. For each LU category, maps depicting the location of grid cells that i) do not share a common dominant LU category across models (white cells), ii) share a common dominant LU category across models but not all models have a fractional coverage > 85% for that LU category (blue cells), or iii) share a common dominant LU category across models and all models have a fractional coverage > 85% for that LU category (red). Results show are for the EUR domain. The number of blue and red cells is shown as insert in each map. No maps are shown for the deciduous needleleaf forest, evergreen broadleaf forest, mixed forest, shrubland, herbaceous, savanna, wetlands, tundra, and snow and ice LU categories because there is not a single common dominant LU grid cell across models for these categories (see Table 5).

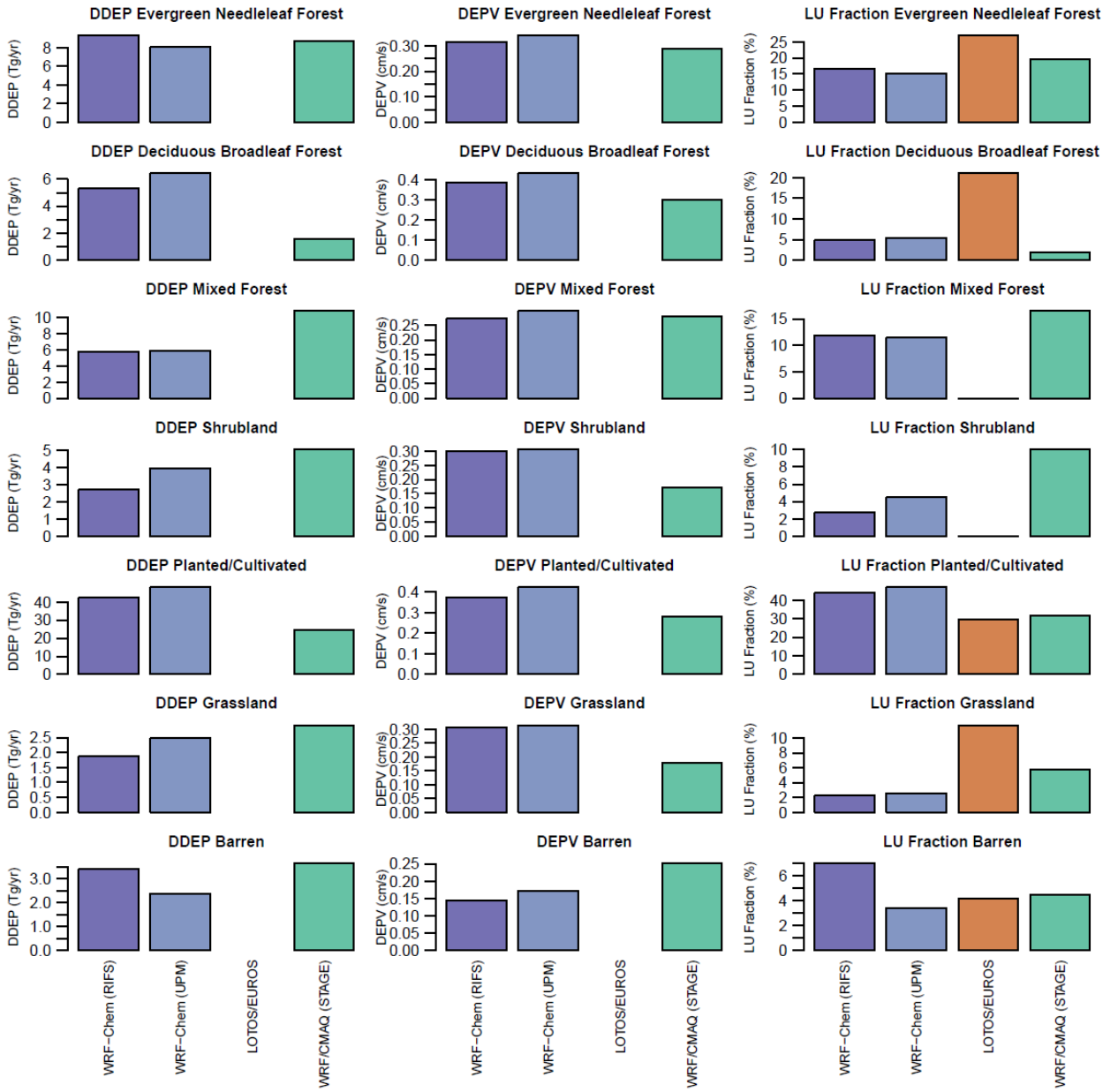

Figure S16. LU-specific annual domain-total dry deposition fluxes (Tg), LU-specific annual mean dry deposition velocity (cm/s), and percentage LU category domain coverage (excluding water grid cells) for seven selected LU categories over the EUR domain. For each LU category and model, the analysis considered grid cells in the analysis domain common to all models in which a given model had at least 85% coverage for this LU category. The number of these grid cells differs across models due to underlying differences in LU (see Section 3.3).

References

Broxton, P. D., Zeng, X., Sulla-Menashe, D., and Troch, P. A.. A global land cover climatology using MODIS data. Journal of Applied Meteorology and Climatology, 53(6), 1593-1605. DOI: 10.1175/JAMC-D-13-0270.1, 2014

Clifton, O. E., Schwede, D., Hogrefe, C., Bash, J. O., Bland, S., Cheung, P., Coyle, M., Emberson, L., Flemming, J., Fredj, E., Galmarini, S., Ganzeveld, L., Gazetas, O., Goded, I., Holmes, C. D., Horváth, L., Huijnen, V., Li, Q., Makar, P. A., Mammarella, I., Manca, G., Munger, J. W., Pérez-Camanyo, J. L., Pleim, J., Ran, L., San Jose, R., Silva, S. J., Staebler, R., Sun, S., Tai, A. P. K., Tas, E., Vesala, T., Weidinger, T., Wu, Z., and Zhang, L.: A single-point modeling approach for the intercomparison and evaluation of ozone dry deposition across chemical transport models (Activity 2 of AQMEII4), Atmos. Chem. Phys., 23, 9911–9961, https://doi.org/10.5194/acp-23-9911-2023, 2023

EEA. (2020). CLC 2012—Copernicus Land Monitoring Service [Dataset]. Retrieved from https://land.copernicus.eu/pan-european/corine-land-cover/clc-2012

Friedl, M. A., McIver, D. K., Hodges, J. C. F., Zhang, X. Y., Muchoney, D., Strahler, A. H., Woodcock, C. E., Gopal, S., Schneider, A., Cooper, A., Baccini, A., Gao, F., and Schaaf, C. Global land cover mapping from MODIS: Algorithms and early results. Remote Sensing of Environment, 83(1–2), 287–302. Https://doi.org/10.1016/S0034-4257(02)00078-0, 2002

Makar, P. A., Akingunola, A., Aherne, J., Cole, A. S., Aklilu, Y.-A., Zhang, J., Wong, I., Hayden, K., Li, S.-M., Kirk, J., Scott, K., Moran, M. D., Robichaud, A., Cathcart, H., Baratzedah, P., Pabla, B., Cheung, P., Zheng, Q., and Jeffries, D. S.: Estimates of exceedances of critical loads for acidifying deposition in Alberta and Saskatchewan, Atmos. Chem. Phys., 18, 9897–9927, https://doi.org/10.5194/acp-18-9897-2018, 2018.

Zhang, L., Brook, J. R., and Vet, R.: A revised parameterization for gaseous dry deposition in air-quality models, Atmos. Chem. Phys., 3, 2067–2082, https://doi.org/10.5194/acp-3-2067-2003, 2003